AIAA-2005-1094
AIAA 43rd Aerospace Sciences Meeting & Exhibit
Reno, NV, January, 2005

Separated Turbulent Flow Simulations Using a Reynolds Stress Model and Unstructured Meshes

Emre Alpman* and Lyle N. Long†
Department of Aerospace Engineering
The Pennsylvania State University
University Park, PA, 16802, U.S.A.

Numerical simulation of three-dimensional, separated, high Reynolds number turbulent flows is performed using a second-order accurate cell-centered finite volume method on unstructured meshes. The computations include an application of Reynolds Stress Modeling (RSM), which consists of coupling the Reynolds transport equations with the Favre averaged Navier-Stokes Equations. The resulting system of 12 coupled, non-linear partial differential equations is solved using PUMA_RSM which is an in-house an unstructured grid computational fluid dynamics code written in ANSI-C++. Computations are performed on unstructured meshes composed of tetrahedral cells. In order to reduce the CPU time and memory requirements, parallel processing is applied with the MPI (Message Passing Interface) communication standard. The resulting parallel code is run on Beowulf clusters. Results for high Reynolds number flow around a 6:1 prolate spheroid and a sphere are presented and compared with experimental results. In the prolate spheroid case predictions of mean pressure and circumferential locations of cross flow separation points are in good agreement with experiment. The locations of primary and secondary separation points are computed with an error of roughly three degrees. Mean pressure and skin friction predictions for sphere solutions are also in good agreement with the measurements. The computed separation location is very close to the measured one. The distribution of turbulent stresses shows that the turbulent flow around a sphere is highly anisotropic and supports the notion that using anisotropic turbulence models are necessary for three-dimensional separated flows.

I. Introduction

Separated turbulent flow around three-dimensional geometries is one of the most challenging problems in aerospace. For example, one of the common problems in helicopter fuselage aerodynamics is separated turbulent flow. Flow separates from the hub or fuselage and then impinges on the tail rotor, empennage and control surfaces. Separated flow around a body results in many phenomena in aerodynamics, such as drag increase, lift loss, unsteady fluctuations, etc. Therefore, accurate turbulence prediction is a key to understanding and predicting separated turbulent flows around aerodynamic devices[1]. The presence of three-dimensionality and curvature introduces changes in the turbulence structure, thus invalidating many of the turbulence models widely used for simple and mildly complex shear layers[2]. Therefore, it becomes extremely important to employ more physics in providing suitable closure models for adequate prediction of these complex flows.

Many of the closure models in the literature (e.g. k-ε, k-ω, Spalart-Allmaras, Baldwin-Lomax) are based on the Boussinesq approximation[3]:

$$\tau_{ij} \cong \mu_T \left(\frac{\partial \widetilde{u}_i}{\partial x_j} + \frac{\partial \widetilde{u}_j}{\partial x_i} \right) - \frac{2}{3} \mu_T \frac{\partial \widetilde{u}_k}{\partial x_k} \delta_{ij} \tag{1}$$

which assumes that the principal axes of the Reynolds stress tensor are coincident with those of the mean strain rate at all points in a turbulent flow. For complex three-dimensional flows with sudden changes in mean strain rate the

* Graduate Research Assistant, exa152@psu.edu
† Professor, lnl@psu.edu

Boussinesq hypothesis can be seriously in error because the Reynolds stresses will adjust to such changes at a rate unrelated to mean flow processes and time scales[3]. The Boussinesq approximation also yields the necessity of defining length and time scales of turbulence for eddy viscosity calculations. In zero and one equation models, these scales are defined in an adhoc fashion for different flows. The models are isotropic in nature and are only valid for two-dimensional simple shear flows. Therefore, two-equation models constitute the minimum level of closure that is physically acceptable[3]. Although two-equation models can be superior to zero and one equation models, without modification, they still fail to capture many of the features associated with complex flows[2]. While these models can be modified to improve their predictive accuracy, the modifications are largely adhoc and cannot be easily generalized[3]. Moreover, in the case of strong separation, even the modified two-equation models were shown to fail to predict flow physics due to their isotropic nature[4]. Therefore, anisotropic models such as full Reynolds stress transport models (RSM)[5], are necessary for accurate prediction of three-dimensional separated flows. Although RSM does not represent the unsteady nature of turbulence as does dynamic models such as Large Eddy Simulation (LES)[6], it is very effective in computing the time averaged quantities and requires much less CPU time than LES.

The present work employs RSM for simulation of separated turbulent flows around three-dimensional bodies. The method consists of coupling the transport equations for Reynolds stresses and turbulence dissipation rate[5] with the Favre averaged Navier-Stokes equations[3]. Favre averaging makes it possible to predict the variations in mean density without explicitly modeling the parts related to density variations. The proposed model has been used and validated for various three-dimensional high Reynolds number flows[7-9]. Although the Reynolds stress transport equations are written for time averaged quantities, the method can still be used for unsteady flow simulations when the characteristic frequencies of the phenomenon are sufficiently low compared to the characteristic frequencies of turbulence[10].

II. Methodology

The resulting system of 12 coupled non-linear partial differential equations is numerically solved using the computer code PUMA_RSM, which is an in-house computational fluid dynamics code written in ANSI C++. PUMA_RSM is a modified version of the computer code PUMA2[11-14] which has been used and validated by Long et al. for numerical solution of numerous problems[11-23]. The equations are discretized by a second order finite volume method and solved using an explicit four-stage Runge-Kutta type integration technique. Although explicit methods suffer from limitations on the maximum allowable time step size, they require a minimum number of arithmetic operations per iteration step and are easier to parallelize compared to implicit methods[24].

Solutions around a 6:1 prolate spheroid and a sphere are obtained using unstructured meshes composed of 5.1 million and 3.8 million tetrahedral cells, respectively. The cells are clustered in the vicinity of the solid boundary for sufficient boundary layer resolution. Here the non-dimensional distance $y+$ of the first cells is on the order of one for both cases. Unstructured grids are relatively easy to construct around complex three-dimensional bodies and they offer very efficient cell distributions for accurate solutions of complex real life problems. The sectional views of the computational meshes generated for the problems and a close-up view of the cells near the solid boundary are displayed in Figures 1 and 2.

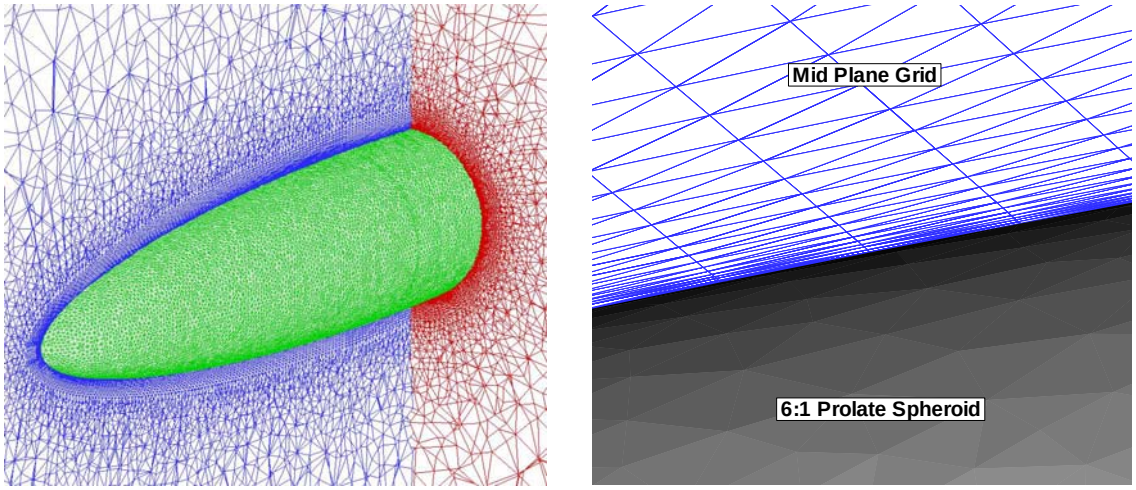

Figure 1 Sectional and close-up views of the cells around a 6:1 prolate spheroid.

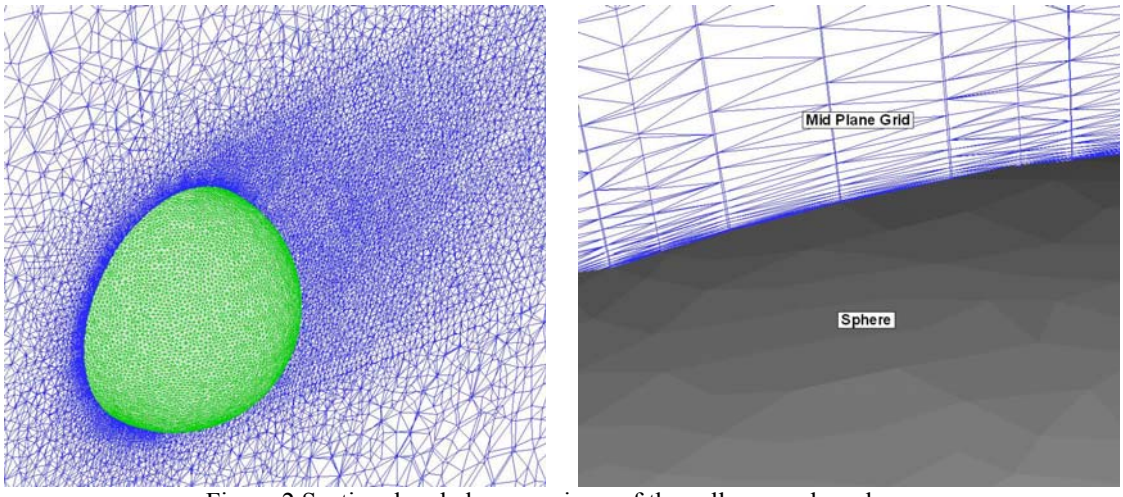

Figure 2 Sectional and close-up views of the cells around a sphere.

Although, in a computational sense, RSM costs much less than LES and DNS; the solutions still require considerable computer resources. The RSM equations have been time averaged, so they are not time dependent. LES and DNS solutions require thousands or millions of time steps. RSM represents a 3-D problem, while LES and DNS are 4-D problems (space and time). But RSM still requires millions of grid cells and parallel processing is applied to reduce the CPU time and memory requirements. The MPI (Message Passing Interface)[25] communication standard is used for this purpose and the code is run on a Beowulf cluster . Our COst Effective Computing Array (COCOA3) is a cluster of off-the-shelf PCs connected via fast ethernet. These PCs run RedHat Linux with MPI[25]. COCOA3 contains 60 2.4 GHz. dual Intel Xeon processors, each having 2 GB of RAM and dual 100 Mbps fast Ethernet cards.

III. Mathematical Formulation

The integral form of the governing equations (RSM) can be written as:

$$\frac{\partial}{\partial t}\int_{\Omega}\mathbf{q}\,d\Omega+\oint_{S}\overline{\overline{F}}\cdot d\mathbf{S}-\oint_{S}\overline{\overline{F}}_{v}\cdot d\mathbf{S}-\oint_{S}\overline{\overline{F}}_{T}\cdot d\mathbf{S}-\int_{\Omega}\mathbf{Q}\,d\Omega=0 \tag{2}$$

where $\mathbf{q}$ is the vector containing the conservative variables, $\overline{\overline{F}}$ is the convective flux tensor, $\overline{\overline{F}}_{v}$ is the viscous flux tensor, $\overline{\overline{F}}_{T}$ is the turbulent flux tensor and $\mathbf{Q}$ is the vector containing turbulent source terms. The conservative variable vector $\mathbf{q}$ can be written as:

$$\mathbf{q}=\left[\overline{\rho}\quad\overline{\rho}\widetilde{u}\quad\overline{\rho}\widetilde{v}\quad\overline{\rho}\widetilde{w}\quad\overline{\rho}\breve{E}\quad\tau_{xx}\quad\tau_{yy}\quad\tau_{zz}\quad\tau_{xy}\quad\tau_{xz}\quad\tau_{yz}\quad\overline{\rho}\varepsilon\right]^{T} \tag{3}$$

where $\overline{\rho}$ is the mean density, $\widetilde{u}$, $\widetilde{v}$, $\widetilde{w}$ are mean velocity components in the *x, y* and *z*-directions, $\breve{E}$ is the total energy per unit mass, τ_{ij} are the Reynolds stresses and ε is the turbulent dissipation rate. In the equations $(\widetilde{\cdot})$ denotes Favre averaging[3], $(\overline{\cdot})$ denotes non-weighted averaging and $(\breve{\cdot})$ denotes an average quantity that is neither a Favre average nor a non-weighted average[8]. Here total energy is different than the Favre averaged total energy which contains turbulent kinetic energy.

$$\breve{E}=\frac{\overline{p}}{\overline{\rho}(\gamma-1)}+\frac{\widetilde{V}^{2}}{2} \tag{4}$$

In Equation (4) $\bar{p}$ is the mean static pressure. The details of the flux tensors and the source vector are as follows:

A. Convective Flux Tensor

$$\bar{\bar{F}} = \begin{bmatrix} \bar{\rho}\tilde{u} & \bar{\rho}\tilde{v} & \bar{\rho}\tilde{w} \\ \bar{\rho}\tilde{u}^2 + \bar{p} & \bar{\rho}\tilde{u}\tilde{v} & \bar{\rho}\tilde{u}\tilde{w} \\ \bar{\rho}\tilde{u}\tilde{v} & \bar{\rho}\tilde{v}^2 + \bar{p} & \bar{\rho}\tilde{v}\tilde{w} \\ \bar{\rho}\tilde{u}\tilde{w} & \bar{\rho}\tilde{v}\tilde{w} & \bar{\rho}\tilde{w}^2 + \bar{p} \\ \bar{\rho}\tilde{u}\breve{H} & \bar{\rho}\tilde{v}\breve{H} & \bar{\rho}\tilde{w}\breve{H} \\ \tilde{u}\tau_{xx} & \tilde{v}\tau_{xx} & \tilde{w}\tau_{xx} \\ \tilde{u}\tau_{yy} & \tilde{v}\tau_{yy} & \tilde{w}\tau_{yy} \\ \tilde{u}\tau_{zz} & \tilde{v}\tau_{zz} & \tilde{w}\tau_{zz} \\ \tilde{u}\tau_{xy} & \tilde{v}\tau_{xy} & \tilde{w}\tau_{xy} \\ \tilde{u}\tau_{xz} & \tilde{v}\tau_{xz} & \tilde{w}\tau_{xz} \\ \tilde{u}\tau_{yz} & \tilde{v}\tau_{yz} & \tilde{w}\tau_{yz} \\ \tilde{u}\bar{\rho}\varepsilon & \tilde{v}\bar{\rho}\varepsilon & \tilde{w}\bar{\rho}\varepsilon \end{bmatrix} \tag{5}$$

where $\breve{H}$ is the total enthalpy per unit mass.

$$\breve{H} = \breve{E} + \frac{\bar{p}}{\bar{\rho}} \tag{6}$$

B. Viscous Flux Tensor

$$\bar{\bar{F}}_V = \begin{bmatrix} 0 & 0 & 0 \\ \bar{t}_{xx} & \bar{t}_{xy} & \bar{t}_{xz} \\ \bar{t}_{xy} & \bar{t}_{yy} & \bar{t}_{yz} \\ \bar{t}_{xz} & \bar{t}_{yz} & \bar{t}_{zz} \\ \bar{t}_{xx}\tilde{u} + \bar{t}_{xy}\tilde{v} + \bar{t}_{xz}\tilde{w} - \bar{q}_x & \bar{t}_{xy}\tilde{u} + \bar{t}_{yy}\tilde{v} + \bar{t}_{yz}\tilde{w} - \bar{q}_y & \bar{t}_{xz}\tilde{u} + \bar{t}_{yz}\tilde{v} + \bar{t}_{zz}\tilde{w} - \bar{q}_z \\ 0 & 0 & 0 \\ 0 & 0 & 0 \\ 0 & 0 & 0 \\ 0 & 0 & 0 \\ 0 & 0 & 0 \\ 0 & 0 & 0 \\ 0 & 0 & 0 \end{bmatrix} \tag{7}$$

where the mean viscous stresses and laminar heat transfer rates are approximated as follows [26]:

$$\bar{t}_{ij} \cong \breve{\mu}\left(\frac{\partial \tilde{u}_i}{\partial x_j} + \frac{\partial \tilde{u}_j}{\partial x_i}\right) - \frac{2}{3}\breve{\mu}\frac{\partial \tilde{u}_k}{\partial x_k}\delta_{ij} \tag{8}$$

$$\overline{q}_i \cong -\breve{K}\frac{\partial \overline{T}}{\partial x_i} \tag{9}$$

C. Turbulent Flux Tensor

$$\overline{\overline{F}}_T = \begin{bmatrix} 0 & 0 & 0 \\ \tau_{xx} & \tau_{xy} & \tau_{xz} \\ \tau_{xy} & \tau_{yy} & \tau_{yz} \\ \tau_{xz} & \tau_{yz} & \tau_{zz} \\ \tau_{xx}\widetilde{u} + \tau_{xy}\widetilde{v} + \tau_{xz}\widetilde{w} - q_{Tx} & \tau_{xy}\widetilde{u} + \tau_{yy}\widetilde{v} + \tau_{yz}\widetilde{w} - q_{Ty} & \tau_{xz}\widetilde{u} + \tau_{yz}\widetilde{v} + \tau_{zz}\widetilde{w} - q_{Tz} \\ (d_{xx})_1 & (d_{xx})_2 & (d_{xx})_3 \\ (d_{yy})_1 & (d_{yy})_2 & (d_{yy})_3 \\ (d_{zz})_1 & (d_{zz})_2 & (d_{zz})_3 \\ (d_{xy})_1 & (d_{xy})_2 & (d_{xy})_3 \\ (d_{xz})_1 & (d_{xz})_2 & (d_{xz})_3 \\ (d_{yz})_1 & (d_{yz})_2 & (d_{yz})_3 \\ (d_{\varepsilon})_1 & (d_{\varepsilon})_2 & (d_{\varepsilon})_3 \end{bmatrix} \tag{10}$$

where (d_{ij}) and (d_{ε}) are diffusion terms for Reynolds stresses and turbulent dissipation term, respectively. Here the diffusion of Reynolds stresses is modeled using the triple correlations model of Hanjalic and Launder[27].

$$(d_{ij})_n = -C_s\frac{k}{\varepsilon}\left[\tau_{im}\frac{\partial \tau_{jn}}{\partial x_m} + \tau_{jm}\frac{\partial \tau_{in}}{\partial x_m} + \tau_{nm}\frac{\partial \tau_{ij}}{\partial x_m}\right] + \breve{\nu}\frac{\partial \tau_{ij}}{\partial x_n} \tag{11}$$

A similar expression is written for the turbulent dissipation rate:

$$(d_{\varepsilon})_n = -C_{\varepsilon}\frac{k}{\varepsilon}\left[\tau_{km}\frac{\partial \varepsilon}{\partial x_m}\right] + \breve{\nu}\frac{\partial \varepsilon}{\partial x_n} \tag{12}$$

Where $C_s = 0.11$, $C_{\varepsilon} = 0.18$. In the above equations, *k* is the turbulent kinetic energy.

$$k = -\frac{1}{2\overline{\rho}}(\tau_{ii}) \tag{13}$$

The turbulent heat transfer rates are approximated using a simple gradient model[8].

$$\overline{q}_{Ti} \cong -\frac{\mu_T C_p}{\mathrm{Pr}_T}\frac{\partial \overline{T}}{\partial x_i} \tag{14}$$

where

$$\mu_T = C_{\mu}\breve{\mu}\,\mathrm{Re}_T \tag{15}$$

$$\mathrm{Re}_T = \frac{\overline{\rho}\, k^2}{\breve{\mu}\, \varepsilon} \tag{16}$$

$$C_\mu = 0.09 \ \exp\left[\frac{-2.5}{\left(1 + 0.02\,\mathrm{Re}_T\right)}\right] \tag{17}$$

Here C_p is the specific heat at constant pressure, Pr_T is the turbulent Prandtl number.

D. Turbulent Flux Tensor

$$\mathbf{Q} = \begin{bmatrix} 0 \\ 0 \\ 0 \\ 0 \\ -P + \overline{\rho}\varepsilon \\ -P_{xx} + \overline{\rho}\varepsilon_{xx} - \phi_{xx} \\ -P_{yy} + \overline{\rho}\varepsilon_{yy} - \phi_{yy} \\ -P_{zz} + \overline{\rho}\varepsilon_{zz} - \phi_{zz} \\ -P_{xy} + \overline{\rho}\varepsilon_{xy} - \phi_{xy} \\ -P_{xz} + \overline{\rho}\varepsilon_{xz} - \phi_{xz} \\ -P_{yz} + \overline{\rho}\varepsilon_{yz} - \phi_{yz} \\ S \end{bmatrix} \tag{18}$$

where P_{ij} is the exact production term due to mean strain rates[5]:

$$P_{ij} = \tau_{ik}\frac{\partial \widetilde{u}_j}{\partial x_k} + \tau_{jk}\frac{\partial \widetilde{u}_i}{\partial x_k} \tag{19}$$

The dissipation tensor $\overline{\rho}\,\varepsilon_{ij}$ is approximated using local isotropy assumption[3]

$$\overline{\rho}\,\varepsilon_{ij} = \frac{2}{3}\overline{\rho}\,\varepsilon\,\delta_{ij} \tag{20}$$

The ϕ_{ij} term in Equation (18) is the pressure redistribution term. This term is the most important item in the closure because it controls both the separation and reattachment processes[7-10]. The term is split into slow and rapid parts[3] and their corresponding wall echo terms which arise from the reflection of pressure fluctuations from the rigid wall[28]. The slow and the rapid terms are modeled as follows[29]:

$$\phi_{ij,1} \cong -C_1\overline{\rho}\,\varepsilon\left(-\frac{\tau_{ij}}{\overline{\rho}\,k} - \frac{2}{3}\delta_{ij}\right) \tag{21}$$

$$\phi_{ij,2} \cong -C_2\left(P_{ij} - \frac{1}{3}P_{mm}\delta_{ij}\right) \tag{22}$$

The models for slow[30] and rapid[29] wall echo terms are displayed in the following equations:

$$\phi_{ij,1}^{w} \cong -C_1^{w} \frac{\varepsilon}{k}\left[\tau_{km} n_k n_m \delta_{ij} - \frac{3}{2}\tau_{ki} n_k n_j - \frac{3}{2}\tau_{kj} n_k n_i\right] f \tag{23}$$

$$\phi_{ij,2}^{w} \cong C_2^{w}\left[\phi_{km,2} n_k n_m \delta_{ij} - \frac{3}{2}\phi_{ki,2} n_k n_j - \frac{3}{2}\phi_{kj,2} n_k n_i\right] f \tag{24}$$

where $\boldsymbol{n}$ is the surface normal. Near wall damping function f is taken as $0.4k^{3/2}/\varepsilon y_n$, y_n being the normal distance to the wall. The coefficients $C_1, C_2, C_1^{w}, C_2^{w}$ are optimized by Launder and Shima[28]. Finally the source term S is given by the following relation[3]:

$$S = C_{\varepsilon 1}\frac{\varepsilon}{k}\tau_{ij}\frac{\partial \tilde{u}_i}{\partial x_j} - C_{\varepsilon 2}\,\bar{\rho}\frac{\varepsilon\,\varepsilon^{*}}{k} \tag{25}$$

where ε^{*} is the modified dissipation rate which goes to zero at the solid wall[28].

IV. Numerical Method

The governing equations are numerically solved using an unstructured grid finite volume technique, which employs a Lax-Friedrich scheme[31] for convective fluxes and space centered scheme for viscous and turbulent fluxes. The resulting semi-discrete equations are numerically integrated using a four stage Runge-Kutta integration technique with local time stepping to enhance the convergence to steady state. The solution of the equations requires appropriate time steps limited by the stability bound of the scheme. The local time step is computed through stability analyses for the inviscid convection, viscous diffusion, turbulent diffusion and turbulent dissipation. At the solid boundaries a no slip condition is applied where all the velocity components, as well as the Reynolds stresses, are set to zero. The turbulent dissipation rate at the wall is computed using Equation (26).

$$\varepsilon_w = 2\breve{\nu}\left(\frac{\partial\sqrt{k}}{\partial n}\right)^2 \tag{26}$$

Where n is the distance normal to the wall. The solid boundaries are also assumed to be adiabatic. Although time averaged quantities are solved for, the governing equations are assumed to be time dependent for iterative purposes. Therefore, they require initial conditions. In this study the freestream conditions are used for the initial velocity and density. Pressure is computed using the equation of state. Freestream turbulence is assumed to be isotropic. For the prolate spheroid solutions the characteristic freestream velocity of turbulence is assumed to be 0.03% of the mean speed[32] while this value is taken as 0.45% for the sphere results. The turbulent dissipation rate is then computed assuming that the freestream length scale for large eddies is 0.1 m [10].

V. Results and Discussion

Results for high Reynolds number flow around a 6:1 prolate spheroid and a sphere are presented here

A. Results for a 6:1 Prolate Spheroid

For the numerical solution the freestream Reynolds number, freestream Mach number and flow angle of attack are taken to be $6.5\text{x}10^6$, 0.1322 and 30 degrees, respectively. The solutions required 13.04 GB of memory and took nearly 8 days on 30 COCOA3 processors. Figure 3 shows the pressure distribution of the midplane and comparison with experimental data[33]. The predictions show good agreement with measurements except at the extreme aft end of the spheroid. The main reason for this discrepancy is the numerical dissipation of the vortical flowfield. Vortices move away from the body to coarser grid region as they travel along the longitudinal direction.

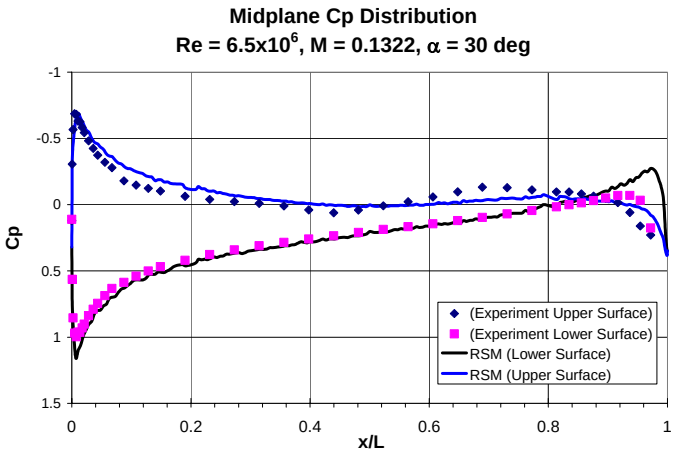

Figure 4 Midplane Cp distribution of a 6:1 prolate spheroid.
Re = 6.5x10^6, M = 0.1322, α = 30°.

Three-dimensional separation is both difficult to model and poorly understood. Unlike two-dimensional separation, three-dimensional separation is rarely associated with the vanishing of the wall shear stress[32]. The flow around a prolate spheroid separates on the lee side of the body and forms a surface that rolls into a vortex. Thus, skin friction lines on either side of the separation converge asymptotically toward the separation line[34]. At high angles of attack secondary separation might occur at a higher circumferential angle. Such behavior can be easily observed from Figure 5 where the vorticity contours at different axial stations are displayed along with the surface skin friction lines.

It is clear from Figure 5 that the skin friction lines asymptotically converge toward a separation line. Vortex formation is also evident at the aft portions of the body just after this separation line. At the upper lee side of the body a second separation line is also observed. Predicted primary and secondary separation locations at the axial station $x/L = 0.738$ are tabulated and compared with measurements[33] in Table 1.

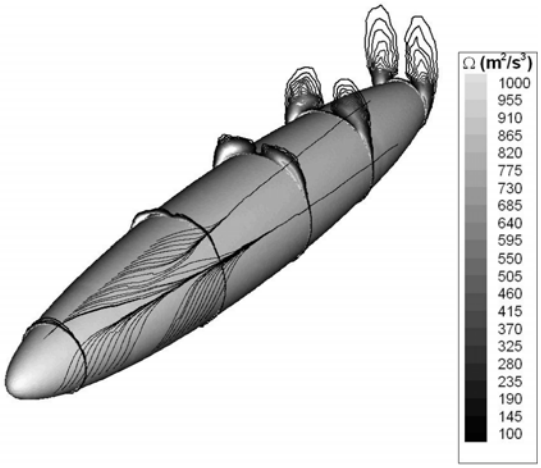

Figure 5 Vorticity contours at different axial locations with surface skin friction lines.
Re = 6.5x10^6, M = 0.1322, α = 30°.

Table 1. Primary and Secondary Separation Locations, $x/L = 0.738$
$Re = 6.5x10^6$, $M = 0.1322$, $\alpha = 30°$.

	RSM Solution	Measurement
Circumferential Location of Primary Separation [degrees]	~ 105	~ 108
Circumferential Location of Secondary Separation [degrees]	~ 159	~ 156

The predictions are very close to the experimental data. The discrepancy is approximately three degrees for both cases. Another indication of three-dimensional separation is the in the vicinity of the separation point near the wall[34]. Figure 6 shows the longitudinal velocity contours at axial station $x/L = 0.738$. Two localized minimum regions (darker regions) can be observed from this figure. These regions are close to the measured primary and secondary separation points.

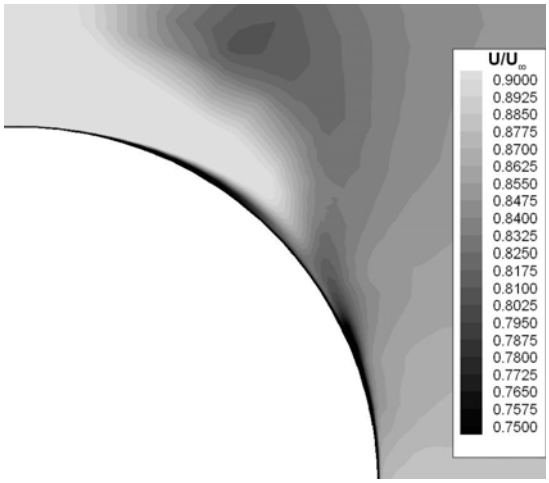

Figure 6 Longitudinal velocity contours, $x/L = 0.738$.
$Re = 6.5x10^6$, $M = 0.1322$, $\alpha = 30°$.

For a more detailed analysis, the circumferential distribution of longitudinal velocity, predicted at a distance of 0.14 cm from the wall, is plotted in Figure 7. In the figure local minima occur at circumferential locations of 112 and 151 degrees which are very close to the measured primary and secondary separation points.

Figure 8 shows the lateral skin friction distribution at $x/L = 0.738$ and comparison with the measurements[33]. Predictions show qualitative agreement with experiment. The skin friction coefficient is difficult to measure and experimental data always contain some uncertainities[34]. In addition to this, accurate skin friction coefficient computation in unstructured grid with skewed cells is also very difficult. But qualitative agreement is still good and encouraging.

The prolate spheroid results clearly showed that RSM can be effectively used for the predictions of three-dimensional separated flows where the models based on Boussinesq approximation would most likely fail due to their isotropic nature. In addition, LES solutions would require thousands or millions of timesteps. The RSM numerical solutions successfully represented the physics of the problem. The primary and even the secondary separation location were predicted accurately with approximately three degrees of discrepancy from the experiment.

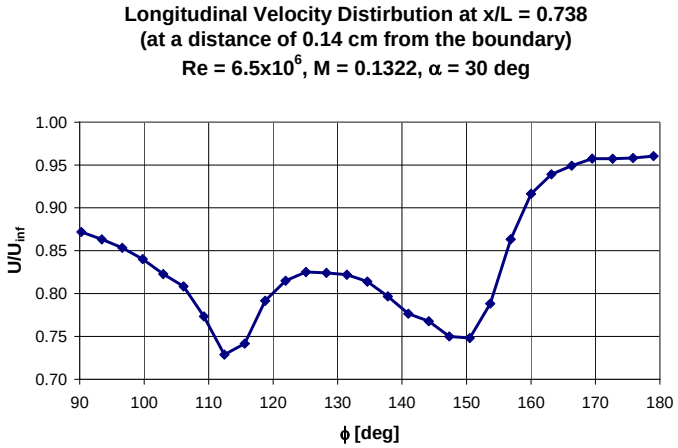

Figure 7 Circumferential distribution of longitudinal velocity at 0.14 cm away from the wall, *x/L* = 0.738. Re = 6.5x10^6, M = 0.1322, α = 30°.

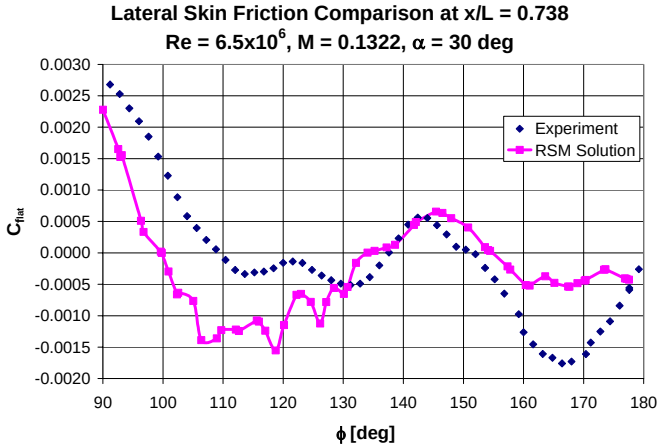

Figure 8 Skin friction distribution, *x/L* = 0.738. Re = 6.5x10^6, M = 0.1322, α = 30°.

B. Results for a Sphere

For the sphere solution, the freestream Reynolds number and freestream Mach number are taken to be 1.14x10^6 and 0.1763, respectively. The solution required 9.72 GB of memory and took nearly 7 days on 30 COCOA3 processors. Figure 9 shows the circumferential pressure distribution and comparison with experimental data[35]. The results are in very good agreement with the measurements with slight discrepancies between 90 and 120 degrees. Such discrepancies were also observed by the LES solutions in Ref. 6.

As in the prolate spheroid case, flow separation is analyzed by plotting skin friction lines and the circumferential skin friction distribution. Figure 10 shows the skin friction lines along with the velocity contours and Figure 11 shows the circumferential skin friction distribution and comparison with the measurements[35].

It is clear from Figure 10 that the skin friction lines stop at a circumferential angle of approximately 120 degrees, which indicates the separation location. Boundary layer thickening beyond this point is also evident from the velocity distribution contours. The predicted separation location is very close to the experimental value[35]. This is also supported by Figure 11 where the computed skin friction coefficient is in very good agreement with the experiment[35] with some discrepancies in the vicinity of 90 degrees. These differences are due to laminar-turbulent transition which is not modeled by the current numerical method.

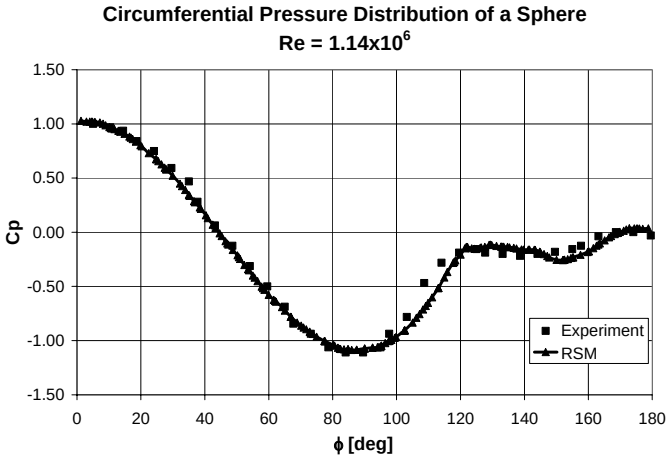

Figure 9 Circumferential Cp distribution of a 6:1 prolate spheroid.
Re = 1.14x10^6, M = 0.1763.

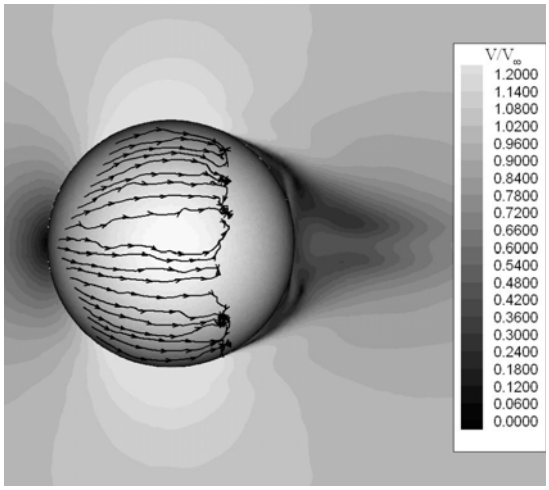

Figure 10 Velocity distribution with surface skin friction lines
Re = 1.14x10^6, M = 0.1763.

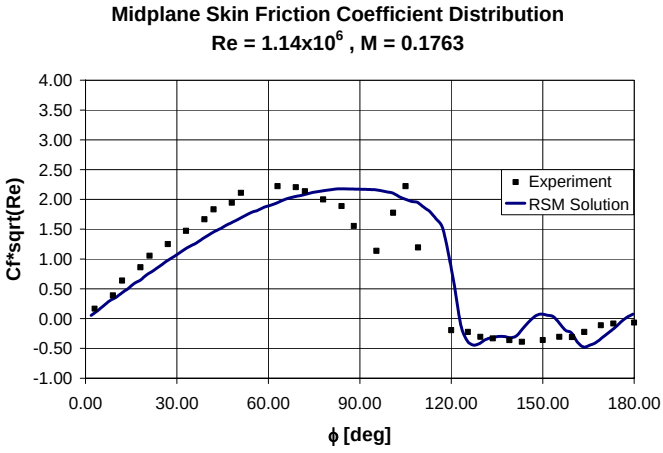

Figure 11 Circumferential skin friction distribution.
Re = 1.14x10^6, M = 0.1763.

Taneda[36], through his flow visualizations suggested a mechanism for vortex shedding in the wake of a sphere. He observed that a vortex sheet separating from the sphere forms a pair of strong streamwise vortices. Such a behavior is observed in Figure 12 which shows a time averaged iso-vorticity surface. This structure was also observed in the LES results by Jindal et al [6].

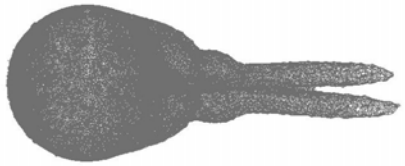

Figure 12 Iso-vorticity surface in the wake of a sphere
$Re = 1.14 \times 10^6$, M = 0.1763.

In order to analyze the turbulent structure of the flow, normalized τ_{xx} and τ_{xz} distributions are plotted and displayed in Figures 13 and 14. Normalization is preformed by dividing the quantity by mean density and turbulent kinetic energy. In isotropic turbulence, normalized τ_{xx} and τ_{xz} take the values of 2/3 and 0 respectively. The large deviations from these values mean non-isotropy is present in the turbulence structure. It is clear from these figures that the flow is highly anisotropic. The figures clearly support the notion of employing anisotropic turbulence models, such as RSM, for accurate prediction of three-dimensional separated flows.

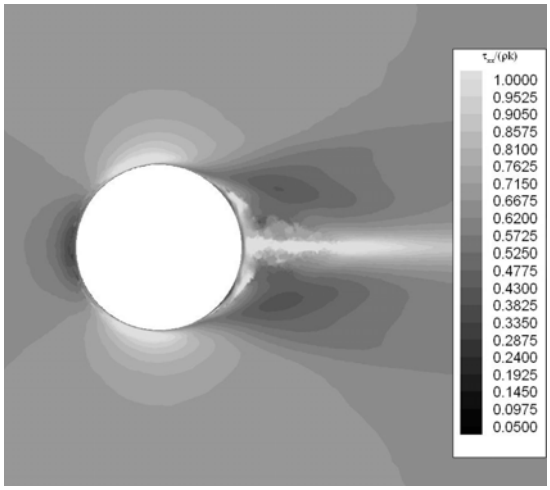

Figure 13 Normalized τ_{xx} contours
$Re = 1.14 \times 10^6$, M = 0.1763.

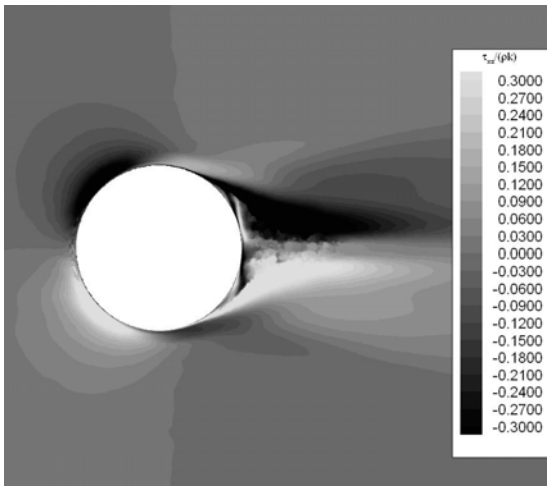

Figure 14 Normalized τ_{xz} contours
$Re = 1.14x10^6$, M = 0.1763.

VI. Conclusion

High Reynolds number separated turbulent flows around a 6:1 prolate spheroid and a sphere were predicted using RSM. The model consists of a numerical solution of the Favre averaged Navier-Stokes equations coupled with the transport equations for Reynolds stresses and the turbulent dissipation rate. The prolate spheroid solution was performed at a Reynolds number of $6.5x10^6$, Mach number of 0.1322 and flow angle of attack of 30 degrees. Results were encouraging and showed good agreement with experiments. The behavior of the surface skin friction lines and crossflow separation point at $x/L = 0.738$ were consistent with experimental data. The predicted locations of the primary and secondary separation were within three-degrees of the measurements. The sphere solution was performed at a Reynolds number of $1.14x10^6$, and a Mach number of 0.1763. The sphere results were also in good agreement with the measurements. Slight discrepancies were observed between the computed and measured skin friction coefficients, which are mainly due to the laminar-turbulent transition. Analysis of the normalized turbulent stresses revealed that the turbulent structure of the flow was highly anisotropic. This supported the necessity of employing anisotropic turbulence models for three-dimensional separated flows.

Results clearly showed that RSM can handle three-dimensional separated flows where most of the eddy viscosity models would be insufficient. Since the model is not flow dependent it can be employed for other geometries (including complex shapes) and flow conditions.

References

[1] Souliez, F. J., "Parallel Methods for Computing Unsteady Separated Flows Around Complex Geometries," Ph.D. Thesis, Aerospace Engineering Department, Penn State University, State College, PA, 2002.

[2] Lakshminarayana, B., "Turbulence Modeling for Complex Shear Flows," *AIAA Journal*, Vol.24, No. 12, 1986, pp 1900 – 1917.

[3] Wilcox, D. C., *Turbulence Modeling for CFD*, DCW Industries Inc, ISBN 1-928729-10-X.

[4] Slomski, J. F., Gorski, J. J., Miller R. W., Marioni T. A., "Numerical Simulation of Circulation Control Airfoils as Affected by Turbulence Models," *AIAA 40th Aerospace Sciences Meeting & Exhibit*, AIAA 2002-0851, Reno, NV, January 2002.

[5] Launder, B. E., Reece, G. J., Rodi W., "Progress in the Development of a Reynolds-Stress Closure," *Journal of Fluid Mechanics*, Vol. 68, No. 3, pp. 537 – 566, 1975.

[6] Jindal, S., Long. L. N., Plassmann, P. E., Sezer-Uzol, N., "Large Eddy Simulations on a Sphere Using Unstructured Grids," *AIAA Fluid Dynamics Conference and Exhibit*, AIAA 2004-2228, Portland, OR, 2004.

[7] Gerolymos, G. A., Vallet, I., "Wall-Normal-Free Reynolds Stress Closure for Three-Dimensional Compressible Separated Flows," *AIAA Journal*, Vol. 39, No. 10, 2001, pp 1833 – 1842.

[8] Gerolymos, G. A., Vallet, I., "Wall-Normal-Free Reynolds Stress Model for Rotating Flows Applied to Turbomachinery", *AIAA Journal*, Vol. 40, No. 2, 2002, pp 199 – 207.

[9] Chassaing, J. C., Gerolymos, G. A., Vallet, "Efficient and Robust Reynolds-Stress Model Computation of Three-Dimensional Compressible Flows," *AIAA Journal*, Vol. 41, No. 5, 2003, pp 763 – 773.
[10] Chassaing, J. C., Gerolymos, G. A., Vallet, "Reynolds-Stress Model Dual-Time Stepping Computation of Unsteady Three-Dimensional Flows," *AIAA Journal*, Vol. 41, No. 10, 2003, pp 1882 – 1894.
[11] Modi, A., Long, L. N., Sezer-Uzol, N., Plassmann P., "Scalable Computational Steering System for Visualization of Large-Scale CFD Simulations," *Journal of Aircraft* (to be published).
[12] Souliez, F., Long, L., N., Morris, P. J., Sharma, A., "Landing Gear Aerodynamic Noise Prediction using Unstructured Grids," *International. Journal of Aeroacoustics*, Vol. 1, No. 2, 2002
[13] Modi, A., "Unsteady Separated Flow Simulations Using a Cluster of Work Stations," M.S. Thesis, Aerospace Engineering Department, Penn State University, State College, PA, 1999.
[14] Modi, A., Long, L. N., "Unsteady Separated Flow Simulations using a Cluster of Workstations," *38th AIAA Aerospace Sciences Meeting & Exhibit*, AIAA 2000-0272, Reno, NV, January, 2000.
[15] Hansen, R. P., Long, L. N., Large Eddy Simulation of a Circular Cylinder on Unstructured Grids," *40th AIAA Aerospace Sciences Meeting & Exhibit* AIAA 2002-0982, Reno, NV, January 2002.
[16] Alpman, E., Long, L. N., and Kothmann, B. D., "Understanding Ducted Rotor Antitorque and Directional Control Characteristics, Part I: Steady State Simulation," *Journal of Aircraft*, Vol. 41, No. 5, 2004, pp. 1042 – 1053.
[17] Alpman, E., Long, L. N., and Kothmann, B. D., "Understanding Ducted Rotor Antitorque and Directional Control Characteristics, Part I: Unsteady Simulation," *Journal of Aircraft* (to be published)
[18] Modi, A., Long, L. N., Plassmann, P. E. , "Real-Time Visualization of Wake-Vortex Simulations using Computational Steering and Beowulf Clusters," *VECPAR*, Portugal, June 2002.
[19] Long, L. N., Modi, A., "Turbulent Flow and Aeroacoustics Simulations using a Clusters of Workstations," *NCSA Linux Revolution Conference*, IL, June, 2001.
[20] Sharma, A., Long, L. N., "Airwake Simulations on an LPD 17 Ship," *15th AIAA CFD Conference*, AIAA 2001-2589, Anaheim, CA, June 2001.
[21] Long, L. N. Souliez F., Sharma, A., "Aerodynamic Noise Prediction using Parallel Methods on Unstructured Grids," *7th AIAA/CEAS Aeroacoustics Conference*, AIAA 2001-2196, Maastricht, Netherlands, May 2001.
[22] Schweitzer. F., "Computational Simulation of Flow around Helicopter," M.S. Thesis, Aerospace Engineering Department , Penn State University, State College, PA, May, 1999.
[23] Hansen R., "Separated Turbulent Flow," Ph.D. Thesis, Mechanical Engineering Department, Penn State University, State College, PA, August, 2001.
[24] Alpman, E., "Numerical Simulation of Rotary wing Flowfields in Parallel Computers," M.S. Thesis, Aerospace Engineering Department, Middle East Technical University, Ankara, Turkey, July 2001.
[25] Pacheco, P. S., *Parallel Programming with MPI*, Morgan Kaufmann Publishers Inc., 1997.
[26] Vandromme, D., Ha Minh H., "About Coupling of Turbulence Closure Models with Averaged Navier-Stokes Equations," *Journal of Computational Physics*, Vol. 65, 1986, pp. 386 – 409.
[27] Hanjalic, K., Launder B. E., "A Reynolds Stress Model of Turbulence and Its Applications to Thin Shear Flows," *Journal of fluid Mechanics*, Vol. 52, 1972, pp. 609 – 638.
[28] Launder, B. E., Shima. N., "Two-Moment Closure for the Near-Wall Sublayer: Development and Application," *AIAA Journal*, Vol. 27, No. 10 1989, pp. 1319 – 1325.
[29] Gibson, M. M., Launder B. E., "Ground Effects on Pressure Fluctuations in the Atmospheric Boundary Layer," *Journal of Fluid Mechanics*, Vol. 86, 1978, pp. 491 – 511.
[30] Shir, C. C., "A Preliminary Numerical Study of Atmospheric Turbulent Flows in the Idealized Planetary Boundary Layer," *Journal of Atmospheric Sciences*, Vol. 30, 1973, pp. 1327 – 1339.
[31] Hirsch C., *Numerical Computation of Internal and External Flows, Vol. 2: Computational Methods for Inviscid and Viscous Flows*, John Wiley & Sons, 1988.
[32] Chesnakas, C. J., Simpson R.L., "Detailed investigation of the Three-Dimensional Separation About a 6:1 Prolate Spheroid," *Journal of Fluid Mechanics*, Vol. 3, No. 6, pp. 990-999, June 1997.
[33] Kreplin, H. P., Volmers H., Meier H. U., "Shear Stress Measurements on an Inclined Prolate Spheroid in the DFVLR 3 m x 3 m Low Speed Wind Tunnel, Gottingen – Data Report," DFVLR Rept, IB 222-84 A 33, 1985.
[34] Wetzel, T. G., Simpson R. L., Chesnakas, C. J., "Measurement of Three-Dimensional Crossflow Separation," *AIAA Journal*, Vol. 36, No. 4, 1998, pp 557 – 564.
[35] Achenbach, E., "Experiments on the Flow past Spheres at very High Reynolds Numbers," *Journal of Fluid Mechanics*, Vol. 54, No. 3, 1972, pp. 565 – 575.
[36] Taneda, S., "Experimantal Investigations of the Wake Behind a Sphere at Low Reynolds Numbers," *Journal of Physics Japan*, Vol. 11, No. 10, 1956, pp. 1104 – 1108.